The International Journal of Advanced Manufacturing Technology (2021) 113:1255–1266
https://doi.org/10.1007/s00170-021-06682-7

ORIGINAL ARTICLE

Performance analysis of the longitudinal-torsional ultrasonic milling of Ti-6Al-4V

Yu Pang [1,2] · Pingfa Feng [1,3] · Jianjian Wang [3,4] · Huiting Zha [1] · Jie Xu [1,5]

Received: 22 August 2020 / Accepted: 19 January 2021 / Published online: 2 February 2021

Abstract

Titanium alloy is a typical difficult-to-cut material due to its high strength and high stiffness. To solve the problem of the low efficiency and poor surface quality in the milling of titanium alloy, this paper proposes a novel longitudinal-torsional ultrasonic vibration milling (LTUVM) process. An ultrasonic horn with spiral slots was designed to convert the longitudinal vibration into longitudinal-torsional vibration. The tooltip trajectory was modeled, and the finite elements analysis was used to analyze the cutting mechanism of LTUVM. The simulation results indicate a kind of separation cutting characteristics in every vibration cycle, which is beneficial to reduce the cutting force and improve the surface finish compared with the single longitudinal ultrasonic vibration milling (SLUVM). Then, cutting tests were conducted on Ti-6Al-4V to evaluate the performance of LTUVM. Experimental results demonstrated that the LTUVM could reduce the cutting force by 46–86% compared with the conventional milling (CM) and the SLUVM due to its separation cutting characteristics. Moreover, the surface morphology was analyzed, and a fractal dimension (FD) method was proposed to characterize the regularity and fragmental property of the machined surfaces. The surface morphology analysis results showed that the LTUVM can be used as a novel high-efficiency and high-quality surface texturing method for Ti-6Al-4V. The textured surface of the LTUVM has the superiority of high integrity and periodicity, which could be applied to effectively tune the tribological property of surface.

Keywords Titanium alloy · Longitudinal-torsional ultrasonic milling · Cutting force · Surface texturing · Microstructures

1 Introduction

Ti-6Al-4V (TC4) alloy is a kind of metallic material with high strength, high stiffness, great corrosion resistance, and other excellent properties. These outstanding properties make it a widely used material in the aerospace field, especially in jet engine compressors and turbine discs [1–3]. However, TC4 is a typical difficult-to-cut material [4], reflected by (1) its low thermal conductivity and high cutting temperature; (2) high tooltip stress; (3) low elastic modulus and severe workpiece spring back; and (4) high chemical activity at high temperature, which results in extreme tool wear. Because of these drawbacks, TC4 alloy machining often encounters problems of low processing efficiency, poor surface quality, and short tool life in industrial production [5].

In recent years, single longitudinal ultrasonic vibration milling (SLUVM) has been applied to machine TC4. Compared with the conventional milling (CM), the SLUVM is a non-traditional machining method that applies a longitudinal vibration to the milling process. Maurotto et al. [6] applied an ultrasonic vibration load to a cutting tool during TC4 cutting, and the cutting force was reduced significantly compared with the CM. Patil et al. [7] explained this phenomenon experimentally and found improvements in surface quality with the SLUVM.

✉ Jianjian Wang
wangjj11@foxmail.com

✉ Huiting Zha
zhahuiting123@sz.tsinghua.edu.cn

[1] Graduate School at Shenzhen, Tsinghua University, Shenzhen 518055, China

[2] Shenzhen Nanshan Foreign Language Senior High School, Shenzhen 518023, China

[3] Department of Mechanical Engineering, Tsinghua University, Beijing 100084, China

[4] Institute of Production Science, Karlsruhe Institute of Technology, 76131 Karlsruhe, Germany

[5] College of Mechanical Engineering, Hunan Institute of Engineering, Xiangtan 411100, China

Apart from the single longitudinal ultrasonic vibration, the longitudinal-torsional ultrasonic vibration has also been introduced into the machining of difficult-to-cut materials. This method uses a discontinuous cutting mode that can reduce the cutting force and cutting heat as well as improve the surface quality and tool life [8, 9]. Wang et al. [10] studied the feasibility of the longitudinal-torsional ultrasonic vibration for the drilling of brittle materials. They reported that the longitudinal-torsional ultrasonic vibration showed an improved performance over the single longitudinal ultrasonic vibration with reduced drilling force and edge chipping defects. Amini et al. [11] investigated the effect of using the longitudinal-torsional ultrasonic vibration on the drilling of Al 7075. They found that the longitudinal-torsional ultrasonic vibration improved the hole quality by reducing the cutting force and changing the tool rake angle.

Inspired by the superiority of longitudinal-torsional ultrasonic vibration in the drilling of difficult-to-cut materials [12, 13], this study is devoted to improving the face milling performance of Ti-6Al-4V (TC4) using the longitudinal-torsional ultrasonic vibration. To achieve the longitudinal-torsional ultrasonic vibration milling (LTUVM), an ultrasonic horn with spiral slots was fabricated and used in the cutting experiments. The cutting performance was evaluated from the cutting simulation results, average cutting force, and surface quality and morphology of the three cutting methods.

2 Development of LTUVM process

2.1 Principle of LTUVM

The cutting principle of the LTUVM is shown in Fig. 1. Compared with the CM, the tooltip trajectory of the LTUVM is applied with ultrasonic vibration in both circumferential and axial direction.

Figure 1 demonstrates that there are longitudinal and torsional harmonic vibrations in Z and X-Y direction, respectively. The trajectory equation of tool tip C_0 in the LTUVM is [14]:

$$\begin{cases} x = r\sin\left(\dfrac{2\pi nt}{60} + \dfrac{A_{\mathrm{T}}}{r}\cos(2\pi ft) + \varphi_0\right) \\ y = r\cos\left(\dfrac{2\pi nt}{60} + \dfrac{A_{\mathrm{T}}}{r}\cos(2\pi ft) + \varphi_0\right) + v_y t \\ z = A_{\mathrm{L}}\sin(2\pi ft) \end{cases} \tag{1}$$

where r is the tool radius, mm; v_y is the feed rate, mm/min; n is the spindle speed, r/min; f is the ultrasonic frequency, Hz; A_T is the torsional amplitude and A_L is the longitudinal amplitude, μm; and φ_0 is the initial angle, rad.

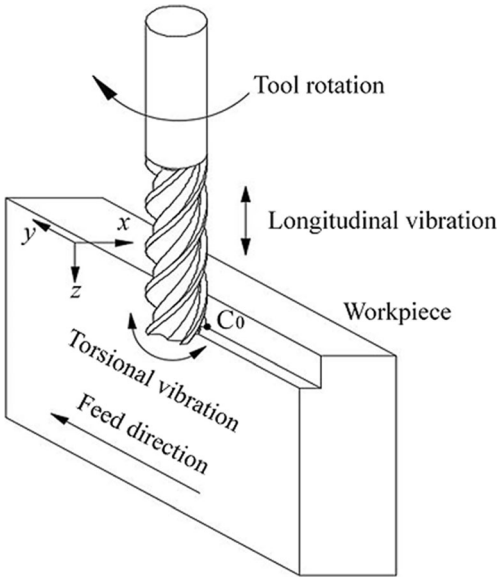

Fig. 1 The principles of the LTUVM

From Eq. (1), the angular velocity w can be expressed by:

$$w = \frac{2\pi n}{60} - 2\pi f\frac{A_{\mathrm{T}}}{r}\sin(2\pi ft) \tag{2}$$

When $2\pi fA_{\mathrm{T}}/r > 2\pi n/60$, the angular velocity w will have periodic negative values, which means that a separation of tooltip cutting takes place at frequency f. If $2\pi fA_{\mathrm{T}}/r < 2\pi n/60$, the cutting will be continuous although the relative velocity between the tool and workpiece varies harmonically. Therefore, the critical rotation speed can be calculated as:

$$n_{\mathrm{crit}} = \frac{60fA_{\mathrm{T}}}{r} \tag{3}$$

The time T that the value of w is negative can be calculated from Eq. (2) as follows:

$$T = \frac{1}{2f} - \frac{1}{\pi f}\arcsin\frac{nr}{60fA_{\mathrm{T}}} \tag{4}$$

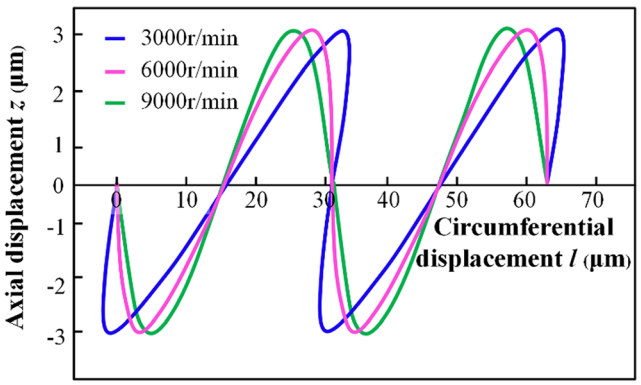

Fig. 2 Effect of rotation speed on tooltip trajectory of the LTUVM

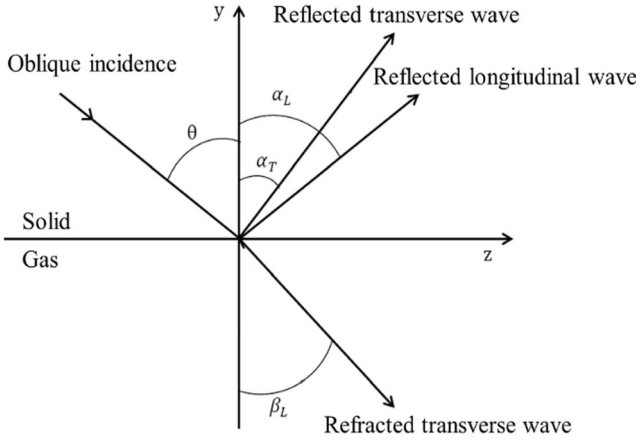

Fig. 3 Wave reflection and refraction on solid-gas interface

Because the torsional vibration of the tooltips is a high-frequency reciprocating motion, it requires the same period to rotate back to a positive value. Thus, the separation time between the tooltip and the workpiece can be expressed by Eq. (5):

$$\Delta T = \frac{1}{f} - \frac{2}{\pi f}\arcsin\frac{nr}{60fA_{\mathrm{T}}} \tag{5}$$

From Eq. (5), it can be found that the parameters that can affect the separation characteristic are n, f, r, and A_{T}. Thus, proper cutting parameters are important to the LTUVM. To study the effect of critical rotation speed, the calculated moving tooltip trajectory in the circumferential direction under different rotation speeds n of LTUVM is shown in Fig. 2. The tooltip path rotates during the cutting process, which makes the tooltip separate from the workpiece periodically. However, after n = 9000 r/min, which equals the critical rotation speed, the path no longer rotates. Therefore, when the rotation speed n exceeds n_{crit}, the separation characteristic will not exist, and the tooltip trajectory will be identical to the longitudinal vibration.

2.2 Design of ultrasonic horn to generate *L–T* vibration

To achieve the LTUVM, this paper utilizes the *L–T* mode conversion method [15, 16]. The mode conversion principle can be explained by oblique incidence theory. When a plane wave is incident with an angle θ onto the solid–gas interface, a reflected transverse wave (α_T), a reflected longitudinal wave (α_L), and a refracted longitudinal wave (β_L) are generated as shown in Fig. 3, which obeys Snell's [17]:

$$\frac{\sin\theta}{c_N} = \frac{\sin\alpha_L}{c_{1L}} = \frac{\sin\alpha_T}{c_{1T}} = \frac{\sin\beta_L}{c_{2L}} \tag{6}$$

where c_{1L} and c_{1T} are the reflected longitudinal and reflected transverse wave speeds in materials, respectively; c_{2L} is the refracted longitudinal wave speed in materials; and c_N is the wave speed of the incident wave.

This paper designed spiral slots on the ultrasonic horn as shown in Fig. 4. Part of the ultrasonic longitudinal waves on the spiral slots was converted to transverse waves, which resulted in mode conversion. Parameters of the spiral slots and ultrasonic horn were determined based on previous results for the *L–T* characteristics of the spiral slots. The horn length is L, the slots position is L_1, the step position is L_2, the input end diameter is D_1, the output end diameter is D_2, the fillet radius is R, the slot length is L_S, and the spiral angle is A. The slot width B was set to 2 mm, the slot depth T was set to 6 mm, and the slot number N was equal to 6. Zhang [18] found that an optimum spiral angle of 52° exists for the spiral slots. The cutting tool was hot-mounted on the ultrasonic horn, and L_3 was the length outside the horn. Its length should be set based on the simulation and testing results.

After modeling a sample ultrasonic horn using the above design parameters, modal and harmonic analyses are carried out using finite elements method (FEM) as shown in Fig. 5. The horn material was 45# steel, its material elastic modulus E was 210GPa, the material density ρ was 7.85 g/cm^3, and Poisson's ratio ν was 0.3. The target frequency was 20 ± 0.5 kHz. Figure 5 shows that the torsional vibration was generated by the longitudinal conversion under its resonant frequency f, which achieved the LTUVM. By changing L_3, different A_{T}, A_{L}, and $A_{\mathrm{T}}/A_{\mathrm{L}}$ could be obtained.

2.3 Evaluation of vibration amplitudes

The LTUVM system is built as shown in Fig. 6. Two types of ultrasonic horns were fabricated with L_3 = 15 mm and L_3 = 20 mm to test their *L–T* vibration characteristics. The horn was

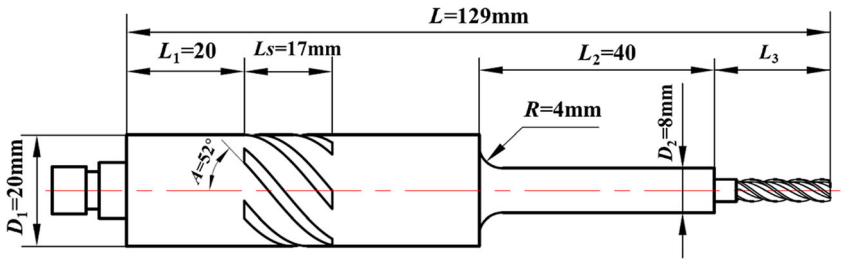

Fig. 4 Structure and parameters of ultrasonic horn with spiral slots

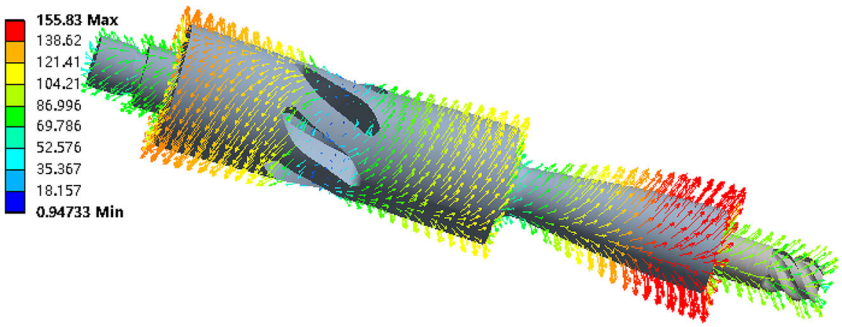

Fig. 5 Resonance mode of the ultrasonic horn with spiral slots

mounted on a threaded connection with a self-developed giant magneto–strictive transducer, which could achieve a large amplitude output [19]. Before the cutting experiment, two ultrasonic horns that were consistent with those used in the experiment were modeled and simulated. The A_T and A_L of the horn were measured by a laser displacement sensor (LK-H008, Keyence, Japan) with a test accuracy of 0.01 μm in the testing experiment.

In order to measure the torsional amplitude, a side plane is milled at the output end of the horn, L is the distance between the side plane to the axis, as shown in Fig. 7a. As the torsional radian θ is small, A_T can be simplified as follows:

$$A_{\mathrm{T}} = R\theta = \frac{RX}{Y} \tag{7}$$

where R is the radius of the cylinder; X is the side plane amplitude; and Y is the height of the measuring point. According to Eq. (7), the torsional vibration amplitude A_T can be derived by measuring X. Detailed information can be found in our previous study [18].

The measurement results are shown in Fig. 7b. The A_T/A_L of the horn where L_3 equals 15 mm is 5 with A_T = 15 μm and A_L = 5 μm, whereas the A_T/A_L where L_3 equals 20 mm is 1.5 with A_T = 3 μm and A_L = 2 μm. The simulation results were consistent with the testing experiments, and the L–T characteristics were better when L_3 was shorter. The former horn had a larger A_T, which equates to a larger critical rotation speed according to Eq. (3). Thus, the ultrasonic horn with L_3 = 15 mm will be used in the cutting tests.

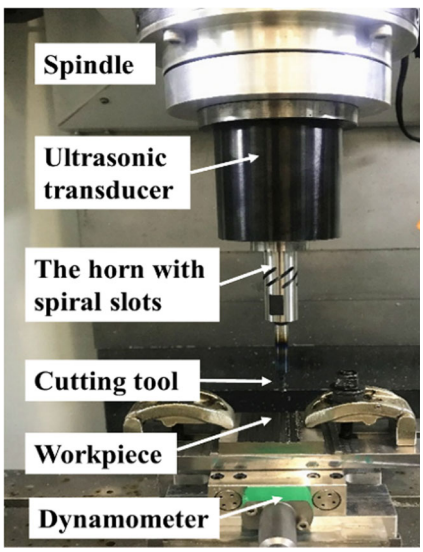

Fig. 6 Mounting of L–T ultrasonic horn

3 Cutting mechanism analysis of LTUVM of Ti-6Al-4V

3.1 Constitutive model of Ti-6Al-4V

The metal cutting process is a multi-factor mechanical model, which needs to consider the influence of strain, strain rate, thermal softening, and other factors. The Johnson–Cook model is used extensively in metal cutting because of its comprehensiveness [20]:

$$\sigma = (A + B\varepsilon^n)\left[1 + C\ln\left(\frac{\dot{\varepsilon}}{\dot{\varepsilon}_0}\right)\right]\left[1 + \left(\frac{T - T_{\mathrm{r}}}{T_{\mathrm{m}} - T_{\mathrm{r}}}\right)^m\right] \tag{8}$$

where A, B, n, C, and m are material constants and T_{r}, T_{m}, σ, ε, $\dot{\varepsilon}$, and $\dot{\varepsilon}_0$ are the room temperature, transition temperature, equivalent flow stress, equivalent plastic strain, equivalent plastic strain rate, and reference strain rate, respectively [21, 22]. The TC4 parameters are given in Table 1.

The Johnson–Cook model is used for material failure. This model is based on the equivalent plastic strain value at the element integral point. The failure process can be divided into two stages: damage failure and damage evolution. The stress–strain relationship of these two stages can be described as:

$$\overline{\varepsilon}^{pf} = \left[d_1 + d_2\exp\left(d_3\frac{\sigma_p}{\sigma_{\mathrm{Mises}}}\right)\right]\left[1 + d_4\ln\left(\frac{\dot{\varepsilon}}{\dot{\varepsilon}_0}\right)\right]\left[1 - d_5\left(\frac{T - T_{\mathrm{r}}}{T_{\mathrm{m}} - T_{\mathrm{r}}}\right)^m\right] \tag{9}$$

where $d_1 - d_5$ represent the failure constants and σ_p and σ_{Mises} are the compressive stress and mises stress, respectively. Refer to Table 2 for $d_1 - d_5$.

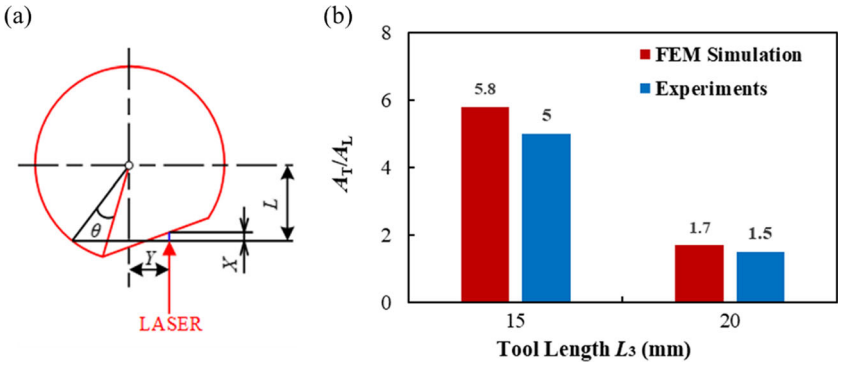

Fig. 7 Testing results of *L*–*T* characteristics

Table 1 Johnson–Cook material parameters [23]

A (MPa)	*B* (MPa)	*C*	*n*	*m*	T_m(°C)	T_r(°C)	$\dot{\varepsilon}_0$ (s^{-1})
1098	1092	0.014	0.93	1.1	1680	20	1

In the finite element model, damage parameter *D* is a measurement factor to judge element failure (element delete). This parameter is based on a cumulative law that is defined as:

$$D = \sum \frac{\Delta \varepsilon^p}{\varepsilon^f} \tag{10}$$

where $\Delta\varepsilon^p$ is the equivalent plastic strain increment and ε^f is the failure strain. When $D = 1$, the element is deleted.

3.2 Development of finite elements model for cutting simulation

The cutting model is established by Abaqus as shown in Fig. 8. The *x* direction represents the main cutting motion direction, and the *z* direction is the feed direction. The thickness *b* is the radial cutting depth which is in the *y* direction, and additional assembly details are provided in Table 3. Table 4 shows the material parameters for the tools and workpiece.

To add the vibration load onto the cutting tools, a periodic amplitude load was applied to the tool velocity. The velocity amplitude *a* can be expressed as:

$$\vec{a} = \overrightarrow{A_0} + \sum_{n=1}^{N} \left[\overrightarrow{A_n} \cos n\omega(t-t_0) + \overrightarrow{B_n} \cos n\omega(t-t_0) \right] \tag{11}$$

where *N* is the number of terms in the Fourier series, ω is the circular frequency, t_0 is the initial moment, $\overrightarrow{A_0}$ is the cutting speed, and $\overrightarrow{A_n}$ and $\overrightarrow{B_n}$ are the maximum amplitude of the longitudinal speed and the torsional speed, respectively. According to the cutting conditions, Eq. (10) can be simplified by using Eq. (11). Table 5 shows the CM, the SLUVM, and the LTUVM settings.

$$\vec{a} = \overrightarrow{A_0} + \vec{A}\cos(n\omega t) + \vec{B}\cos(n\omega t) \tag{12}$$

Table 2 Material damage parameters of Johnson–Cook [24]

d_1	d_2	d_3	d_4	d_5
− 0.09	0.25	− 0.5	0.014	3.87

3.3 Results of cutting simulation

The stress distribution at the same frame in Fig. 9 shows that the LTUVM can effectively reduce the stress concentration and stress value. Although the SLUVM did not reduce the

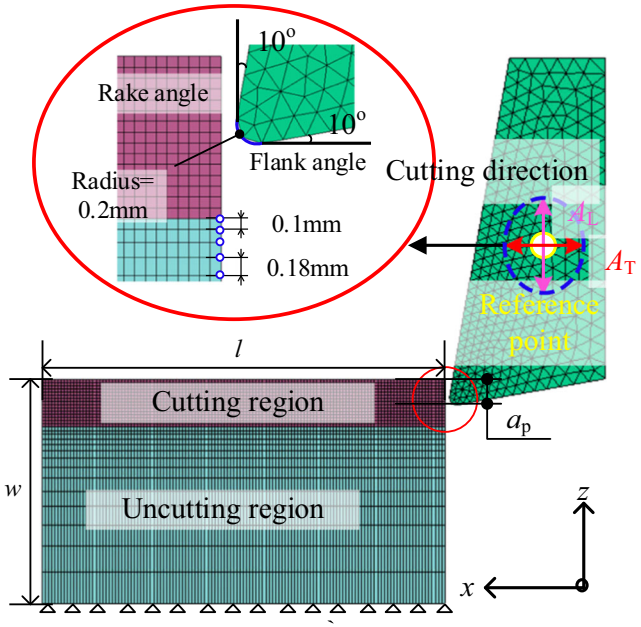

Fig. 8 Finite element geometric model

Table 3 The simulation parameters

Length l (mm)	Cutting depth a_p (mm)	Width of workpiece w (mm)	Workpiece thickness b (mm)	Cutting speed v (mm/s)
12.56	0.5	7	0.5	1000

Table 4 The physical and thermo properties of YG6X and TC4 [23, 25]

Material	Young's modulus E (MPa)	Poisson's ratio ν	Expansion α (m/m·°C)	Density ρ (Ton/m^3)	Specific heat c_p (mJ/Ton·°C))	Thermal conductivity k (W/m·°C)
YG6X	6.35×10^5	0.26	4.70×10^{-6}	14.8×10^{-8}	2.20×10^8	79.6
TC4	1.13×10^5	0.342	9.10×10^{-6}	4.43×10^{-9}	5.46×10^8	7.0

stress concentration, the stress maximum value was reduced slightly compared with the CM. Moreover, the cutting force signal of Fig. 10 demonstrates that the cutting force amplitude of the LTUVM has a periodic cliff-like change, which indicates that the LTUVM is a method of intermittent cutting, whereas the CM and the SLUVM provide continuous cutting. Figure 10 also explains why the average LTUVM force is lower than that of the CM and the SLUVM.

For the average cutting force of the different methods in Fig. 10, the cutting force of the SLUVM is reduced slightly compared with the CM. However, the average cutting force of the LTUVM decreased by 40–50% compared with the CM when the cutting speed was less than 1500 mm/s. When the cutting speed exceeded the critical cutting speed, the LTUVM force reduction is close to that of the SLUVM (see Fig. 11). Thus, the simulation results show the importance of the critical speed and the excellent cutting performance of the LTUVM.

4 Performance evaluation of LTUVM through cutting tests

4.1 Experimental design

The experimental setup is shown in Fig. 12. The LTUVM system was installed onto a five-axes, high-speed vertical machining center (THU ULTRASONIC 850, China). The ultrasonic power supply (BP4610, NF, Japan) could achieve a signal output of 0–150 kHz, and the output voltage peak-to-peak value was 120 V. Trail runs have been conducted to help define the variation range of process parameters. The cutting parameters and L–T characteristic parameters are presented in Table 6 to compare the cutting performance of the CM, SLUVM, and LTUVM. The experiments were conducted three times for each condition, and the average values of process outputs were utilized to present the experimental results.

Table 5 The ultrasonic vibration parameter values

	A (mm/s)	B (mm/s)	f (kHz)	ω (rad/s)	A_L (μm)	A_T (μm)
CM	0	0	20	125600	0	0
SLUVM	376.8	0	20	125600	3	0
LTUVM	376.8	1884	20	125600	3	15

4.2 Measurement method of cutting force and surface morphology

After the cutting experiments in Table 6, A Kistler 9257B dynamometer (Kistler Instrument Corp, Switzerland) is used to record the cutting forces. Two-dimensional (2D) optical

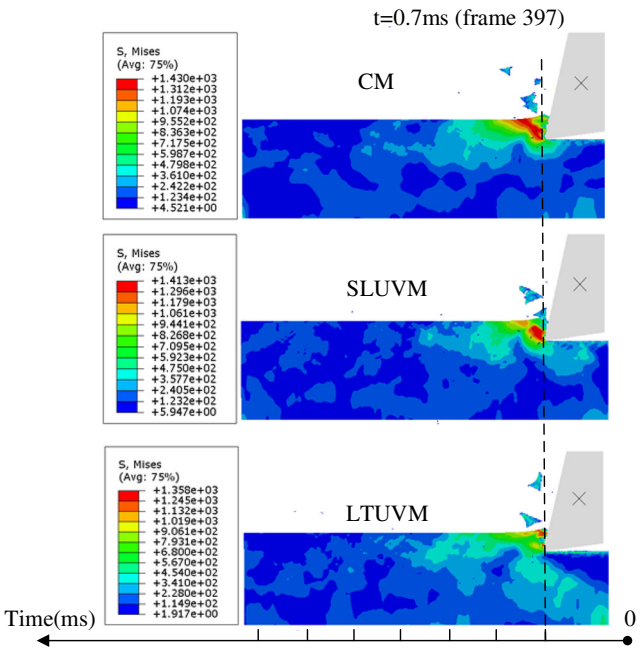

Fig. 9 Stress distribution of the three cutting methods

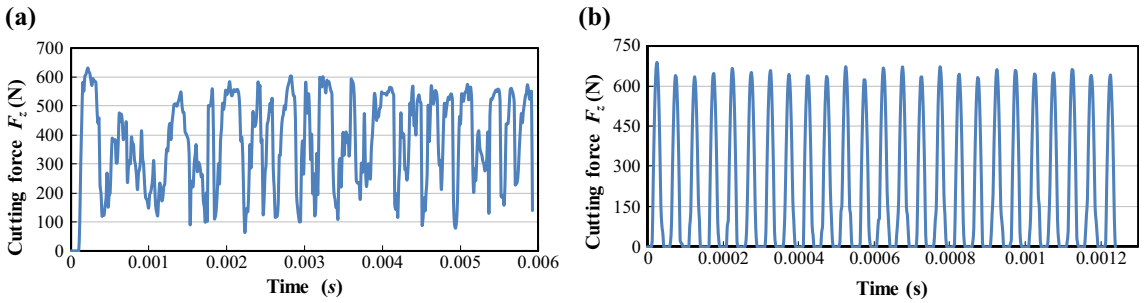

Fig. 10 Cutting force signal of F_z for (**a**) the CM (**b**) the LTUVM

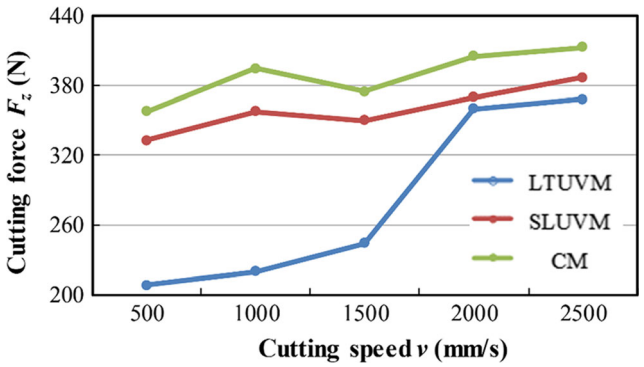

Fig. 11 Cutting force of the three machining methods obtained by cutting simulation

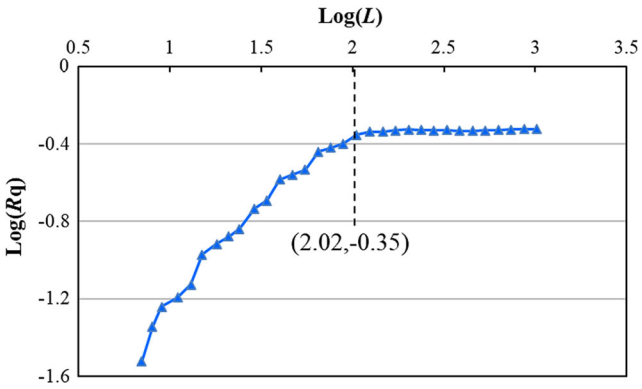

Fig. 13 The curve of R_q~L

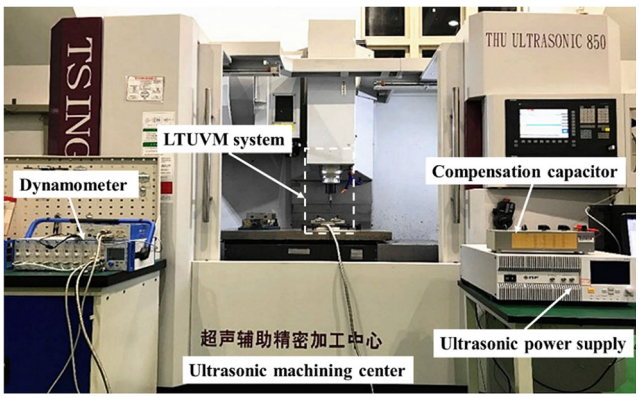

Fig. 12 Setup for cutting tests

photographs and the three-dimensional (3D) morphology of the machined surface are obtained by an electronic speculum and white-light interferometer (WLI) as shown in Fig. 16. The image resolution is 1024 × 1024, and the image size is 337.82 μm × 282.62 μm.

To calculate the surface texture of the LTUVM, 32 points out of 1024 Y direction measurement points in the form of a geometric sequence are taken to draw the R_q~L curve as shown in Fig. 13. It can be seen that the Log (R_q) increases with the increase of Log (L). However, there exits an obvious inflection point at (2.02, − 0.35) which is 105th point out of 1024 measurement points. When the Log (L) exceeds 2.02, the Log (R_q) tends to stay unchanged. The infection point is related to the peak-to-peak value (P_y) of the textured surface. The image size in Y direction is known to be 282.62 μm, so the P_y can be calculated as Eq. (12). The feature size P_y is 29 μm, and the calculated value

Table 6 Experimental cutting parameters and L–T characteristics

Method	Cutting parameters				L–T vibration characteristics			
	n(r/min)	f_z (mm/z)	a_p (mm)	a_n (mm)	f (Hz)	A_L (μm)	A_T (μm)	n_{crit} (r/min)
LTUVM	3000–10000	0.005	0.5	0.5	19780	3	15	9000
SLUVM	3000–10000	0.005	0.5	0.5	19840	3	0	---

is basically the same as the size taken by the electronic speculum in Fig. 16c.

$$\frac{105}{1024} = \frac{P_y}{282.62} \tag{13}$$

In addition, to characterize the surface features, this paper used a measurement of fractal dimension (FD). The FD could reflect the complexity, irregularity, and fragmental property of the surface. A smaller FD yielded a more regular and integrated surface. The FD of a smooth plane equaled to two. The FD that was proposed in fractal geometry is used extensively as a parameter to characterize the topography of engineering surfaces to investigate the self-similar fractal characteristics [26]. The FD is calculated by selecting different measure scales as shown in Fig. 14. As a result, the FD no longer relied heavily on the measure scale and the measuring equipment resolution. In recent years, scholars have discovered that the FD has a power-law relationship with the roughness in machining process [27], which can be expressed as:

$$\begin{cases} R_q = AL^H \\ D_c = 3-H \end{cases} \tag{14}$$

where R_q is the root-mean-square roughness, L is the measure scale, A is the value of Rq under the unit measure scale L, H is the Hurst index, and D_c is the fractal dimensions ($2 < D_c < 3$).

4.3 Experimental results of cutting force

Figure 15 shows the average cutting force for the side milling of TC4 at different spindle speeds, and the cutting force reduction ratio is presented at the top of each figure. Compared with the CM in Fig. 15a, the SLUVM could reduce the cutting force by 8–16%, and the spindle speed did not affect the ratio significantly. However, Fig. 15b illustrates that the LTUVM cutting force was reduced by 46–86% compared with the CM. The main reason for this phenomenon is that the LTUVM has its obvious separation characteristics when $n < n_{crit}$. The cutting force reduction decreased after 9000 r/min which

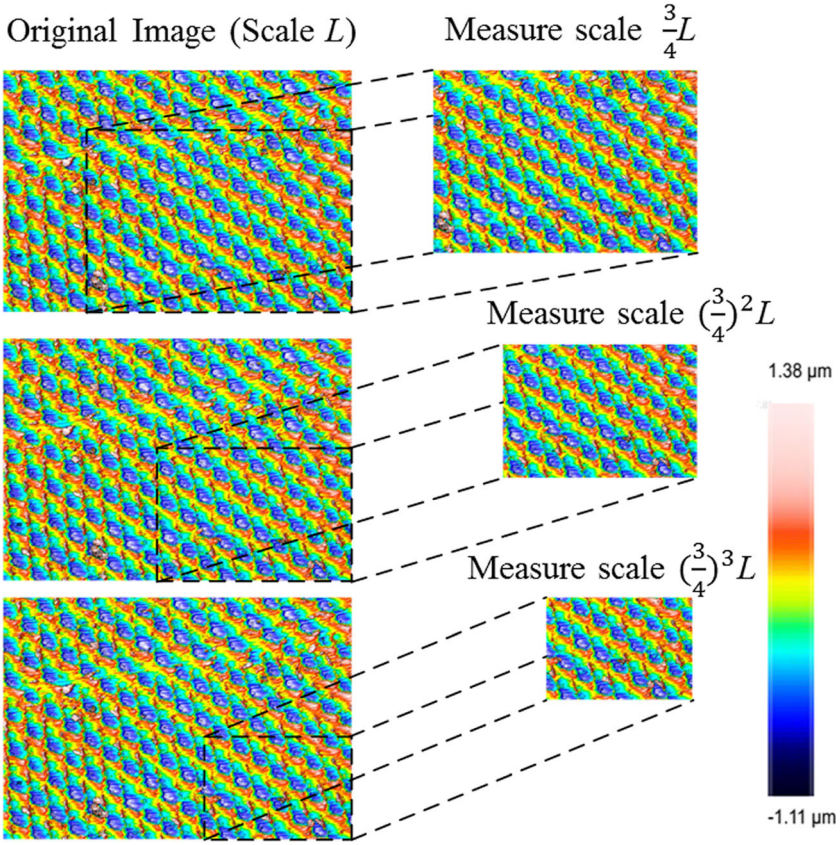

Fig. 14 Principle of FD scaling process

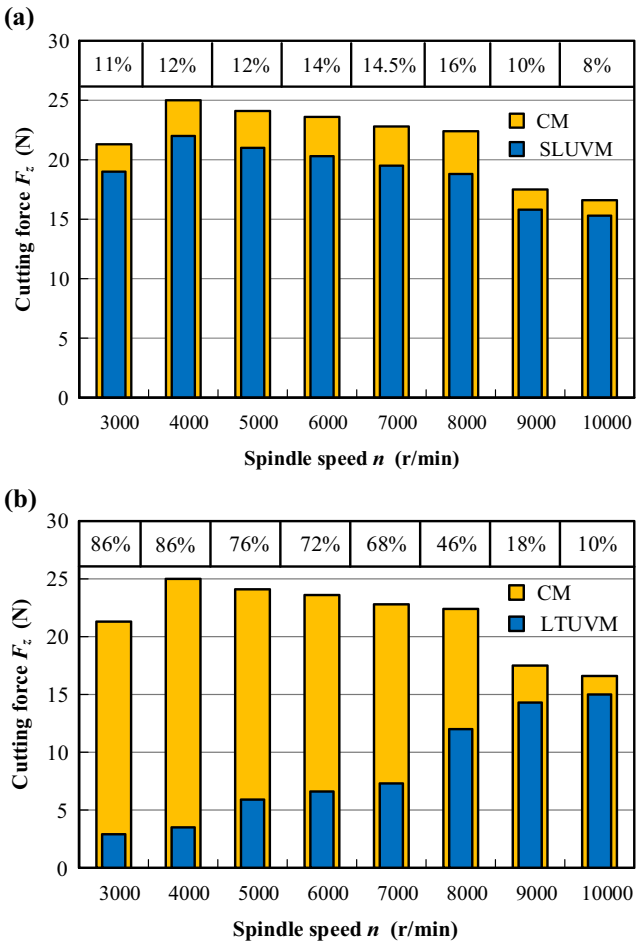

Fig. 15 Cutting force of (**a**) the SLUVM and (**b**) the LTUVM compared with that of the CM. The percentage (%) refers to the cutting force reduction ratio of LTUVM over SLUVM

illustrated that the separation characteristics disappeared. Therefore, the LTUVM became identical to the SLUVM after the critical rotation speed, which is consistent with the trajectory study in Section 2.

4.4 Experimental results of surface morphology

For the convenience of roughness comparison between different milling methods, the value of R_q at the infection point will be used as the roughness of machined surface. Figures 16 and 17 demonstrate the morphology and FD of the finished surfaces that were obtained by different machining methods, respectively. The FD of the CM and the SLUVM was higher than that of the LTUVM, which proves that the surface quality of the LTUVM was better. Moreover, the textured surfaces showed greater potential to improve the tribological performance and friction reductions for further research [28, 29]. The main reason is that the fine and smooth surface morphology can make the friction process reach a stable state more quickly [30, 31]. It could be seen that the LTUVM machined surface had a higher regularity and uniformity compared with that of the CM and the SLUVM. However, the roughness of the LTUVM machined surface is higher shown in Fig. 17 due to the measure scale and limitation of the traditional surface roughness tester.

5 Conclusion

A novel longitudinal-torsional ultrasonic vibration milling (LTUVM) process was developed for the face machining of Ti-6Al-4V. An ultrasonic horn with spiral slots was simulated and designed to achieve effective LTUVM. A theoretical model of the tooltip trajectory of the LTUVM was proposed, after which a cutting simulation based on finite elements model (FEM) was established to analyze the cutting mechanism of LTUVM of Ti-6Al-4V. Then, a series of cutting tests on Ti-6Al-4V were conducted respectively with the conventional milling (CM), the single longitudinal ultrasonic vibration milling (SLUVM), and the LTUVM methods. The average cutting force and machined surface morphology were evaluated. According to the simulation and experiment results, the following conclusions can be drawn:

(1) Based on the theoretical model of the tooltip trajectory in the LTUVM, the critical rotation speed is important in determining whether the tooltip will separate from the workpiece while cutting. When the cutting speed was below the critical cutting speed, the tooltip rotated at an ultrasonic frequency. However, if the cutting speed exceeded the critical speed, the cutting process would be continuous, which was identical to the SLUVM.
(2) The cutting forces by FEM simulation and the experimental results show that the average cutting force of the LTUVM would decrease significantly compared with that of the CM and the SLUVM. The cutting force signal of the LTUVM shows that high-frequency separation between the tool and workpiece occurred periodically below the critical cutting speed, which is the main reason that the average cutting force of the LTUVM was the lowest of the three cutting methods.

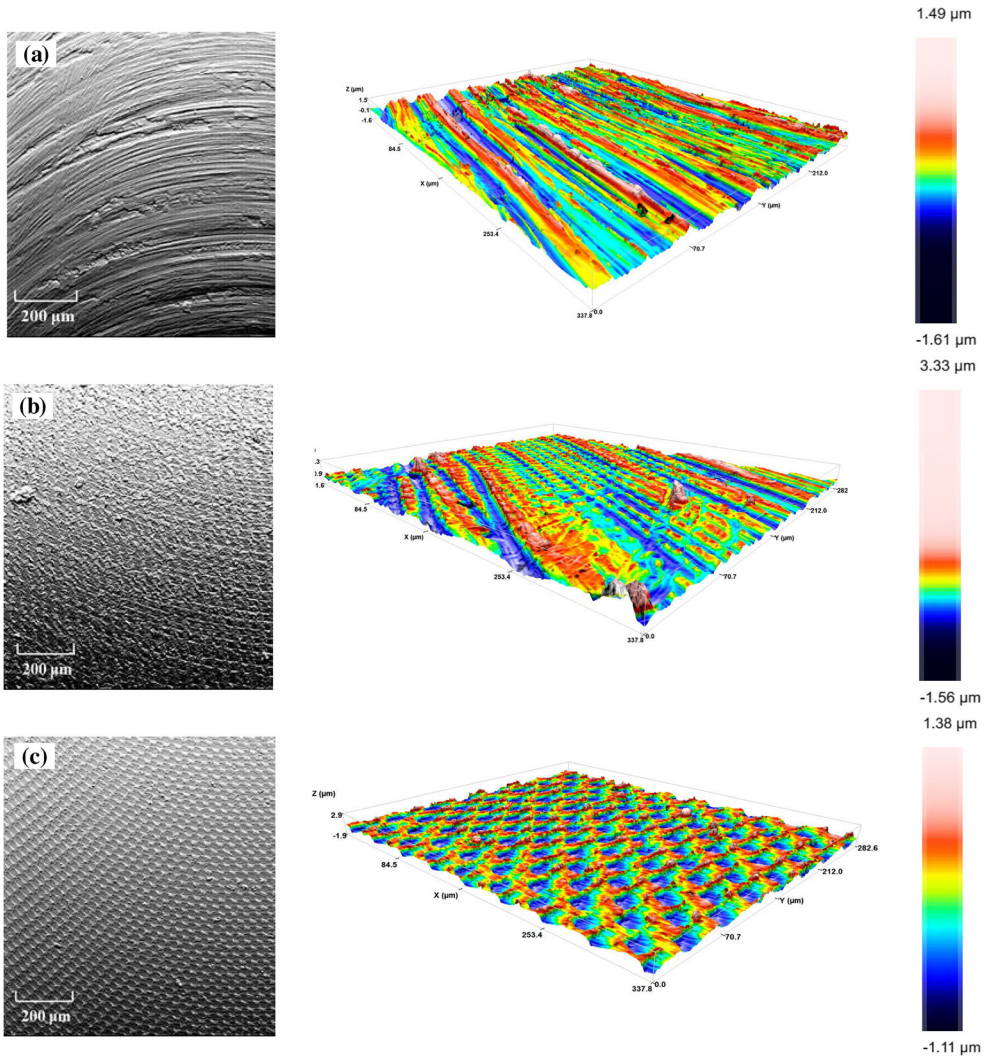

Fig. 16 The 2D and 3D surface topography (**a**) the CM; (**b**) the SLUVM; and (**c**) the LTUVM

(3) Finished surfaces that were obtained by the three cutting methods were analyzed. The 2D topography showed that the LTUVM surface was of great integrity and regularity. Although the surface roughness of the LTUVM was relatively high from longitudinal-torsional vibration addition, the fractal dimension analysis results showed that the machined surface of the LTUVM has higher integrity and periodicity than that of the CM and the SLUVM. It indicates that the LTUVM has the potential to be a novel method for texturing microstructures on the surface of Ti-6Al-4V with the superiority of high efficiency and high quality.

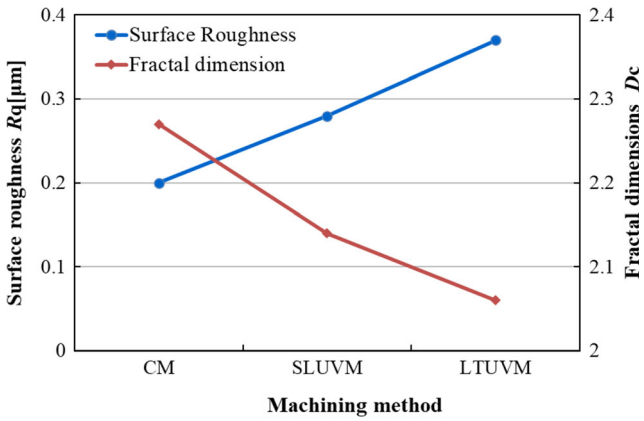

Fig. 17 Quantitative comparison of surface morphology

Authors' contributions Conceptualization, Y.P. and P.F.; methodology, J.W.; validation, Y.P., J.X. and J.W.; investigation, Y.P. and H.Z.; resources, J.X.; supervision, H.Z.; project administration, P.F. All authors have read and agreed to the published version of the manuscript.

Funding This work was supported by National Natural Science Foundation of China [Grant No. 51705281; Grant No. 51875311] and Shenzhen Foundational Research Project (Discipline Layout) [Grant No. JCYJ20180508152128308]. The third author (Jianjian Wang) would like to acknowledge the fellowship support from Alexander von Humboldt Foundation.

Data availability All the data have been presented in the manuscript.

Declarations

Competing interests The authors declare that they have no conflict of interests.

Ethical approval Not applicable.

Consent to participate The authors declare that they all consent to participate this research.

Consent to publish The authors declare that they all consent to publish the manuscript.

References

1. Ellyson B, Brochu M, Brochu M (2017) Characterization of bending vibration fatigue of SLM fabricated Ti-6Al-4V. Int J Fatigue 99: 25–34. https://doi.org/10.1016/j.ijfatigue.2017.02.005
2. Mohsan AUIH, Liu Z, Padhy GK (2017) A review on the progress towards improvement in surface integrity of Inconel 718 under high pressure and flood cooling conditions. Int J Adv Manuf Technol 91(1):107–125. https://doi.org/10.1007/s00170-016-9737-3
3. Umbrello D (2008) Finite element simulation of conventional and high speed machining of Ti6Al4V alloy. J Mater Process Technol 196(1):79–87. https://doi.org/10.1016/j.jmatprotec.2007.05.007
4. Shokrani A, Dhokia V, Newman ST (2016) Investigation of the effects of cryogenic machining on surface integrity in CNC end milling of Ti–6Al–4V titanium alloy. J Manuf Process 21:172–179. https://doi.org/10.1016/j.jmapro.2015.12.002
5. Zhang C, Zhang J, Feng P (2013) Mathematical model for cutting force in rotary ultrasonic face milling of brittle materials. Int J Adv Manuf Technol 69(1):161–170. https://doi.org/10.1007/s00170-013-5004-z
6. Maurotto A, Muhammad R, Roy A, Silberschmidt VV (2013) Enhanced ultrasonically assisted turning of a β-titanium alloy. Ultrasonics 53(7):1242–1250. https://doi.org/10.1016/j.ultras.2013.03.006
7. Patil S, Joshi S, Tewari A, Joshi SS (2014) Modelling and simulation of effect of ultrasonic vibrations on machining of Ti6Al4V. Ultrasonics 54(2):694–705. https://doi.org/10.1016/j.ultras.2013.09.010
8. Chenjun W, Chen S, Cheng K, Xiao C (2019) Investigation of strengthening effect on the machining rigidity in longitudinal torsional ultrasonic milling of thin-plate structures. Proc Inst Mech Eng B J Eng Manuf 234:095440541987534. https://doi.org/10.1177/0954405419875346
9. Ying N, Feng J, Bo Z, Guofu G, Jing-jing N (2020) Theoretical investigation of machining-induced residual stresses in longitudinal torsional ultrasonic–assisted milling. Int J Adv Manuf Technol 108(11):3689–3705. https://doi.org/10.1007/s00170-020-05495-4
10. Wang J, Zhang J, Feng P, Guo P, Zhang Q (2017) Feasibility study of longitudinal-torsional-coupled rotary ultrasonic machining of brittle material. J Manuf Sci Eng 140. https://doi.org/10.1115/1.4038728
11. Amini S, Soleimani M, Paktinat H, Lotfi M (2016) Effect of longitudinal-torsional vibration in ultrasonic assisted drilling. Mater Manuf Process 32:616–622. https://doi.org/10.1080/10426914.2016.1198027
12. Tong J, Zhao J, Chen P, Zhang Z, Zhao B (2019) Effect of ultrasonic longitudinal–torsional composite milling of the residual stress on the surface of titanium alloy. Proc Inst Mech Eng C J Mech Eng Sci 234:095440621989659. https://doi.org/10.1177/0954406219896595
13. Rinck PM, Gueray A, Kleinwort R, Zaeh MF (2020) Experimental investigations on longitudinal-torsional vibration-assisted milling of Ti-6Al-4V. Int J Adv Manuf Technol 108(11):3607–3618. https://doi.org/10.1007/s00170-020-05392-w
14. Gao G, Xia Z, Yuan Z, Xiang D, Zhao B (2020) Influence of longitudinal-torsional ultrasonic-assisted vibration on micro-hole drilling Ti-6Al-4V. Chin J Aeronaut. https://doi.org/10.1016/j.cja.2020.06.012
15. Tsujino J, Ueoka T, Otoda K, Fujimi A (2000) One-dimensional longitudinal–torsional vibration converter with multiple diagonally slitted parts. Ultrasonics 38(1):72–76. https://doi.org/10.1016/S0041-624X(99)00175-4
16. Harkness P, Cardoni A, Lucas M (2009) Ultrasonic rock drilling devices using longitudinal-torsional compound vibration. https://doi.org/10.1109/ULTSYM.2009.5441855
17. Rose JL (2014) Ultrasonic guided waves in solid media. Ultrasonic guided waves in solid media:1–512. doi:https://doi.org/10.1017/CBO9781107273610
18. Zhang Q, Zhang J, Feng P (2019) Characteristics of longitudinal-torsional vibration of ultrasonic horn with slanting slots. J Vib Shock 38(10):63–69+83. https://doi.org/10.13465/j.cnki.jvs.2019.10.009
19. Cai W, Zhang J, Feng P, Yu D, Wu Z (2017) A bilateral capacitance compensation method for giant magnetostriction ultrasonic processing system. Int J Adv Manuf Technol 90(9):2925–2933. https://doi.org/10.1007/s00170-016-9602-4
20. Johnson GR, Cook WH (1983) A constitutive model and data for metals subjected to large strains, high strain rates and high temperatures. In: The 7th International Symposium on Ballistic, Hague, pp 541–547
21. Xu J, Deng Y, Wang C, Liang G (2021) Numerical model of unidirectional CFRP in machining: development of an amended friction model. Compos Struct 256:113075. https://doi.org/10.1016/j.compstruct.2020.113075
22. Ying N, Feng J, Bo Z (2020) A novel 3D finite element simulation method for longitudinal-torsional ultrasonic-assisted milling. Int J Adv Manuf Technol 106. https://doi.org/10.1007/s00170-019-04636-8
23. Xi Y, Bermingham M, Wang G, Dargusch M (2013) FEA modelling of cutting force and chip formation in thermally assisted machining of Ti6Al4V alloy. In: Materials Science Forum, Trans Tech Publications, pp 343–347. https://doi.org/10.4028/www.scientific.net/MSF.765.343
24. Kay (2020) Failure Modeling of Titanium6Al4V and 2024-T3 aluminum with the Johnson-Cook material model. https://doi.org/10.2172/15006359
25. Özel T, Zeren E (2007) Finite element modeling the influence of edge roundness on the stress and temperature fields induced by high-speed machining. Int J Adv Manuf Technol 35(3):255–267. https://doi.org/10.1007/s00170-006-0720-2
26. Feng F, Liu B, Zhang X, Qian X, Li X, Huang J, Qu T, Feng P (2018) Roughness scaling extraction method for fractal dimension evaluation based on a single morphological image. Appl Surf Sci 458:489–494. https://doi.org/10.1016/j.apsusc.2018.07.062
27. Zhang X, Xu Y, Jackson RL (2017) An analysis of generated fractal and measured rough surfaces in regards to their multi-scale structure and fractal dimension. Tribol Int 105:94–101. https://doi.org/10.1016/j.triboint.2016.09.036

28. Kovalchenko A, Ajayi O, Erdemir A, Fenske G, Etsion I (2004) The effect of laser texturing of steel surfaces and speed-load parameters on the transition of lubrication regime from boundary to hydrodynamic. Tribol Trans 47:299–307. https://doi.org/10.1080/05698190490440902
29. Galda L, Sep J, Olszewski A, Żochowski T (2019) Experimental investigation into surface texture effect on journal bearings performance. Tribol Int 136. https://doi.org/10.1016/j.triboint.2019.03.073
30. Chen P, Tong J, Zhao J, Zhang Z, Zhao B (2020) A study ofthe surface microstructure and tool wear of titanium alloys after ultrasonic longitudinal-torsional milling. J Manuf Process 53:1–11. https://doi.org/10.1016/j.jmapro.2020.01.040
31. Li Y, Xiang D, Feng H, Gao G, Shi Z (2020) Surface characteristics investigation of ultrasonic longitudinal-torsional milling of high–volume fraction SiCp/Al. Int J Adv Manuf Technol 110(7):2119–2130. https://doi.org/10.1007/s00170-020-05971-x